Photoneutron Dataset Generation and Analysis at SLEGS*

Zirui Hao,[1,†] Longxiang Liu,[1] Yue Zhang,[1] Hongwei Wang,[1,2,3,‡] Gongtao Fan,[1,2,3,§] Hanghua Xu,[1] Sheng Jin,[2,3] Yuxuan Yang,[2,4] Zhicai Li,[1,5] Pu Jiao,[1,6] Kaijie Chen,[2,7] Qiankun Sun,[2,3] Zhenwei Wang,[2,3] Mengdie Zhou,[1,6] Shan Ye,[1,8] Mengke Xu,[2,3] Xiangfei Wang,[2,3] and Yulong Shen[1,5]

[1]*Shanghai Advanced Research Institute, Chinese Academy of Sciences, Shanghai 201210, China*
[2]*Shanghai Institute of Applied Physics, Chinese Academy of Sciences, Shanghai 201800,China*
[3]*University of Chinese Academy of Sciences, Beijing, 100080, Beijing, China*
[4]*School of Physics, Zhengzhou University, Zhengzhou, 450001, China*
[5]*School of Nuclear Science and Technology, University of South China, Hengyang 421001, China*
[6]*School of Physics, Henan Normal University, Xinxiang 453007, China*
[7]*ShanghaiTech University, Shanghai 201210, China*
[8]*China Institute of Atomic Energy, Beijing, 102413, China*

Photonuclear data are increasingly used in basic research of nuclear physics and application of nuclear technology. The generation of photonuclear data depends on advanced gamma source devices. SLEGS is a new Laser Compton Scattering (LCS) gamma source in Shanghai Synchrotron Radiation Facility (SSRF). It is a crucial beamline for photonuclear reaction cross section measurement and related dataset generation in China. Photonuclear data, including photoneutron, photo-proton, photo-alpha and photo-fission data, as well as the inelastically scattered photon (usually known as nuclear resonance fluorescence (NRF)) data, are useful in nuclear physics, nuclear astrophysics, polarization physics, and other related fields. SLEGS, with its monochromatic characteristics and Laser Compton Slant Scattering (LCSS) mode, offers unique features and methodologies for the measurement and analysis of photonuclear data. This article thoroughly explains the systematic uncertainties of the Flat-Efficiency Detector (FED) system. Additionally, it employs ^{197}Au and ^{159}Tb as case studies to demonstrate the format and processing methods of raw photoneutron data. The content is aimed at the reuse of data analysis.

Keywords: Data descriptor, Raw data, Data repositories, Data sharing, Data reuse

I. INTRODUCTION

Most of the existing photonuclear data are obtained from bremsstrahlung or in-flight positron annihilation gamma sources [1] (for example, Saclay and LLNL Laboratories) and theoretical calculations (TENDL [2], ENDF [3], JENDL [4], and CENDL [5]). The challenge of achieving an accelerator-based gamma source with a single energy has led to a significant scarcity of precise experimental measurements. This has resulted in substantial discrepancies among existing datasets globally. In China, the absence of gamma sources has impeded the acquisition of independent experimental data for photonuclear reaction cross sections, restricting the evaluation and practical application of photonuclear data. For example, nuclear power, a cornerstone of China's sustainable development strategy, underscores the imperative for the design and construction of reactors that are not only safe and efficient, but also stable and reliable. These attributes are crucial for fostering the high-quality growth of China's economy and society. Within nuclear reactors, the presence of numerous high-energy gamma rays initiates photonuclear reactions with reactor materials, leading to the emission of a substantial number of photoneutrons. These photoneutrons might influence the equilibrium and migration of neutrons within the reactor. Consequently, the precise measurement of photonuclear data is paramount for ensuring the safety, efficiency, and reliability of reactor operations, as well as for conducting critical safety assessments and radiation transport analyses.

Furthermore, photonuclear reaction data are vital in basic research of nuclear physics, nuclear analysis, nuclear detection, nuclear diagnosis, and other applied research, such as gamma activation analysis, nuclear safeguard and verification technology, nuclear waste transmutation, human radiotherapy absorbed dose calculation, medical isotope production [6], etc. Accurate photonuclear data measurement is beneficial not only to energy security but also to the health and prosperity of the national economy and people's lives.

The Shanghai Laser Electron Gamma Source(SLEGS) [7–18], a facility based on the principle of Laser Compton Scattering (LCS), serves as a novel gamma-ray source delivering MeV energy γ-ray beams for photonuclear science and technology research. It is one of the 16 beamlines in the Shanghai Synchrotron Radiation Facility (SSRF phase II). SLEGS generates quasi-monochromatic energy-tunable ray beams γ in the energy range of 0.25-21.7 MeV by tuning the interaction angle of laser and electron beam (the corresponding inverse Compton scattering maximum energy is 0.66-21.1 MeV, from 20 to 160 degrees, and 21.7 MeV corresponds to 180 degrees), with a flux of 2.1×10^4-1.2×10^7 photons/s and an energy spread of 5-15% with different collimator apertures. SLEGS energy modification allows it to operate in harmony with other beamline. Its self-adjustability in the interaction

* This work was supported by National Key Research and Development Program of China(No.2022YFA1602404, No.2023YFA1606901), the National Natural Science Foundation of China(No.12275338, No.12388102, No.U2441221), and the Key Laboratory of Nuclear Data Foundation (JCKY2022201C152)
† Corresponding author.Zirui Hao, haozr@sari.ac.cn
‡ Corresponding author.Hongwei Wang, wanghw@sari.ac.cn
§ Corresponding author.Gongtao Fan, fangt@sari.ac.cn

Specifications Table

Subject	Nuclear physics
Specific subject area	Experimental data
Data format	Raw/Analyzed
Type of data	Table and Figure
How data were acquired	Measurements using a Flat-Efficiency Detector (FED) array
Parameters for data collection	Photoneutron cross section data.
Description of data collection	Data were collected by saving list-mode detector array during acquisitions.
Data collection	The data were collected from 2020 using the SLEGS gamma beam and FED array.
Data source location	Institution: Shanghai Advanced Research Institute,CAS Country: China
Data accessibility	Repository name: Science Data Bank Data identification number: https://cstr.cn/31253.11.sciencedb.19543 https://cstr.cn/31253.11.sciencedb.19552 https://cstr.cn/31253.11.sciencedb.19582 Direct URL to data: https://doi.org/10.57760/sciencedb.19543 https://doi.org/10.57760/sciencedb.19552 https://doi.org/10.57760/sciencedb.19582
Related research article	Z.R.Hao, Nuclear Techniques (In Chinese), 43,9(2020). doi:10.11889/j.0253-3219.2020.hjs.43.110501. Z.R.Hao, et al., NIMA:1013 (2021) 165638. doi.org/10.1016/j.nima.2021.165638 H.H.Xu, et al., NIMA1033, 166742(2022). doi:10.1016/j.nima.2022.166742. H.W.Wang, et al., Nucl. Sci.Tech., 33, 87 (2022). doi:10.1007/s41365-022-01076-0. Z.R.Hao, et al., Nucl. Sci. Tech. 35(3), 65 (2024) doi: 10.1007/s41365-024-01425-1. Z.R.Hao, NIMA1068, 169748 (2024).doi:10.1016/j.nima.2024.169748. Z.R.Hao,et al., NIMA1013, 165638 (2021). doi:10.1016/j.nima.2021.165638. L.X.Liu,et al., Nucl.Sci.Tech.,35,111(2024). doi:10.1007/s41365-024-01469-3 L.X.Liu, et al., NIMA1063, 169314 (2024). doi:10.1016/j.nima.2024.169314. Z.C.Li et al., NIMB559(2025) 165595,https://doi.org/10.1016/j.nimb.2024.1655 Z.R.Hao, et al., Science Bulletin (Submitted).

angle can be accomplished in just about 10 minutes, which greatly saves beam time. The SLEGS γ-ray was generated through the interaction between the electron beam from SSRF and a continuous wave (CW) COHERENT DIAMOND Cx-10 (10.6 μm) CO_2 laser[19] at SLEGS laser hutch from Coherent Company. This laser operates flexibly, with a power range of 0.1 to 137 W, a frequency band of 1 to 100 kHz, and adjustable pulse widths from 1 to 1000 μs. The γ-rays are aligned by a Φ (1-30) mm coarse collimator (C), a Φ (1-30) mm fine collimator (F) and a three-hole collimator(T) with apertures of 1 mm, 2 mm, 3 mm. SLEGS officially completed in December 2021 and open to user since January 2023.

Photonuclear data predominantly consist of photoneutron data, which is the main excitation mode of the Giant Dipole Resonance (GDR) of the collective motion of atomic nuclei and the largest part of the excitation function curve. This paper mainly discusses the acquisition and analysis of photoneutron data. SLEGS photoneutron data are currently mainly measured by a Flat Efficiency Detector (FED) array, which consists of 26 sets ^{3}He proportional counters. The collimated γ-rays irradiated the reaction target (usually used Φ (6-10) mm× (0.1-100) mm), which is alignment precisely at the geometric center of the FED. Then the photon-induced neutrons were moderated by polyethylene before being captured by proportional ^{3} He counters. Meanwhile, the residual γ-ray was attenuated by an external copper attenuator and subsequently measured by a large $LaBr_3$ (Φ 3 inch × 4 inch)[21] or BGO detector (Φ 3 inch × 200 mm)[20]. Figure 1 shows the schematic view of the SLEGS beamline.

II. EXPERIMENTAL DESIGN AND DATA GENERATION

The FED is a detector array specifically designed for the measurement of photoneutrons (shown in Fig. 2). It contains 26 sets ^{3}He proportional counters to collect neutrons which embedded in a high-density polyethylene with 500 mm in length, 450 mm in width, and 450 mm in height. This high-density polyethylene is covered on all six sides by 2 mm thick cadmium layers to absorb thermal neutrons from the environment. Additionally, an 50 mm outer layer of polyethylene encapsulates the entire assembly. The center of the moderator is a beam channel with a diameter of 26 mm. The experimental target is placed at the center of the channel. However, Geant4 simulation studies have shown that small changes in target position do not have much effect on neutron measurements. The ^{3}He proportional counters are arrayed into three concentric circles, each positioned at distinct radial distances from the center: 65 mm, 110 mm, and 175 mm. The inner Ring (R1) comprises 6 counters, each with a 1-inch diameter and a length of 500 mm. The middle Ring (R2) contains 8 counters, each 2 inches in diameter and also 500 mm in length. The outer Ring (R3) is equipped with 12 counters, identical to the middle ring's 2-inch diameter and 500 mm length. Collectively, these 26 counters are filled with ^{3}He gas at a pressure of 2 atm.

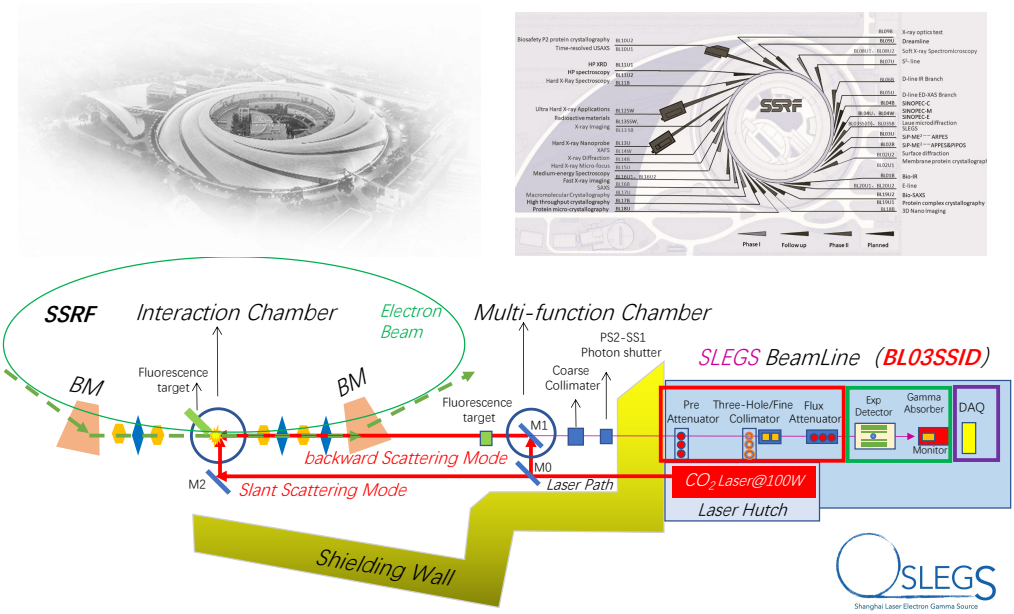

Fig. 1. (Color online) The schematic view of SLEGS beamline in SSRF.

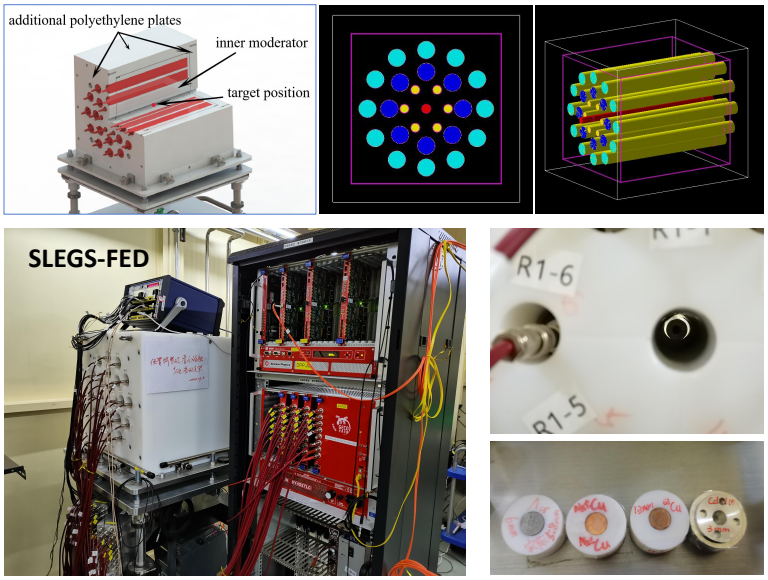

Fig. 2. (Color online) The setup of FED array, including Geant4 simulation, data acquisition(DAQ), 26 sets of ^{3}He proportional counters, pre-amplifier, high-voltage power supply, etc.

The high-voltage of ^{3}He proportional counters is about 1 kV (950 V in R1 and 1050 V in R2&R3), provided by CAEN's A1589 module [23] in SY4527LC [24] High Voltage Power crate. The preamplifier is a 16-channel integrated module developed with the support of a grant. Taking into account the long decay time characteristic of ^{3}He proportional counters, the design incorporates a truncation of the waveform, causing the output signal to decay rapidly after reaching its peak, which used to minimize the dead time of the system.

Digital conversion using Mesytec's MDPP-16 [25] and

MVME [26] Data Acquisition System (DAQ). The MDPP-16 is a regular data acquisition, internally solidified with firmware programs, Standard Charge Integrating Preamplifier (SCP), Peak sensing ADC (PADC), and other programs, which can directly convert the collected waveform data into digital output such as amplitude or area. In the MDPP-16, the output pulses from the charge-sensitive preamplifier are first subjected to gain modification and low-noise amplification before converted to a 80 MHz ADC, and the analog signal is converted to a digital signal and sent to the FPGA firmware for signal reconstruction. The reconstructed signal uses the built-in trapezoidal filtering and fast-time filtering algorithm to obtain the energy and time information. The MVME data acquisition system captures data in a compressed binary format, necessitating decompression and conversion into the ROOT[22] format using specialized code before analysis. The MVME data is archived in '*.zip' files, which contain the raw data in '*.mvlclst' format, an MVME Analysis file named 'analysis.analysis', a log file 'messages.log', and a notes file 'mvme_run_notes.txt'. The binary raw data '*.mvlclst' can be directly decoded by MVME. However, MVME is not suitable for detailed analysis. Consequently, We have developed a decoding program to transform the binary file to the ROOT format according to the MDPP-16 manual [25]. The resulting ROOT file contains a single TTree named 'Tree;1', which includes branches for ADC (signal pulse height); Ch (channel number of MDPP-16), Flag (indicator for pile-up, overflow, or underflow events); Mod (MDPP-16 identifier, with two MDPP-16 modules in total); TDC (signal timestamp); CFD (TDC time difference); dt (time intervals between adjacent events), and EvN (debugging variable; a value of 0 signifies normal conditions). The ADC is utilized for neutron Q-spectra analysis. Ch and Mod are employed to determine the origin of the signal. TDC is used for period analysis and coincidence analysis in the DNM sorting for (γ, xn) (x=2, 3, ...) measurements.

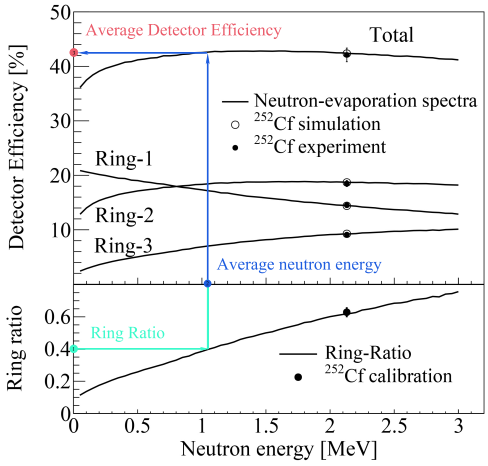

Fig. 3. (Color online) The detector efficiency and RR curve. The RR technique is shown in color lines.

All measurements were performed using a ready-to run, platform independent and open-source DAQ software package MVME which includes hardware configuration, run control as well as online monitoring. A screen of the MVME interface and an operational block diagram are shown in Fig.4. Most of the hardware settings which are programmed in to the matching VME registers are pre-configured, which allows a short learning curve. To achieve high data rates, the MVME software takes advantage of the list sequencer mode of the MVLC controller. Online data monitoring and visualization includes a three-level analysis which allows calibration and basic calculations such as sums, ratios, etc. and 1D/2D histogramming. A built in script language allows creation of plug-in processes, which can do complex data manipulation. Data rates of up to 50 MBytes per second can be stored. For the MDPP-16 this means: with 5 channels responding simultaneously in one event, a rate of 1 MHz can be registered while measuring amplitude and timing.

The FED data acquisition system, consists of four main parts. The first part is the data acquisition control interface, the main functions are to start or stop data acquisition, set the MVLC connection mode with data acquisition electronics, select whether to record data, set the time of data acquisition, set the name of the file of data recording, and select whether the file of recording data is divided by time period or file size. The second part is the VME electronic parameter configuration interface, the main function is to set the two MDPP-16 waveform digital samplers used to obtain and use, set their addresses to be consistent with the settings on the hardware, set the firmware mode to be consistent with the settings on the hardware, and set the integral and derivative time, forming amplification time, rise time, attenuation time and so on of the time filtering of the signal. The third part is the data analysis interface, the main function is to select the data source to be analyzed, perform the necessary logical operations, and generate a visual one-dimensional or two-dimensional histogram. The fourth part is the log interface, the main function is the output of information in the process of data acquisition operation, such as the time when the acquisition is started, the configured electronic parameters, the time when the acquisition is stopped, etc., if there is an error in the acquisition process, it will be displayed in red text on this interface, and the reason for the error can be found through these information.

The BGO or $LaBr_3$ detector for measuring γ-ray is also powered by A1589 module. Pulses from BGO or $LaBr_3$ are digitized by DT5730B and use CoMPASS as the DAQ, operating normally in PHA (Pulse Height Analysis) mode. The data is directly output in CERN root format. In a typical root file, there is only one Tree named Data_R. For preliminary data processing, three Branches are usually used: Channel indicates which channel of the DT5730B the signal was acquired from. Generally, there is only one γ detector placed on the beam line, so only one Channel has data. It is customary to use Channel 1 for $LaBr_3$ signals and Channel 3 for BGO signals. Timestamp is the time stamp of the signal, with units of picoseconds. The Branch named Energy represents the pulse amplitude of the signal.

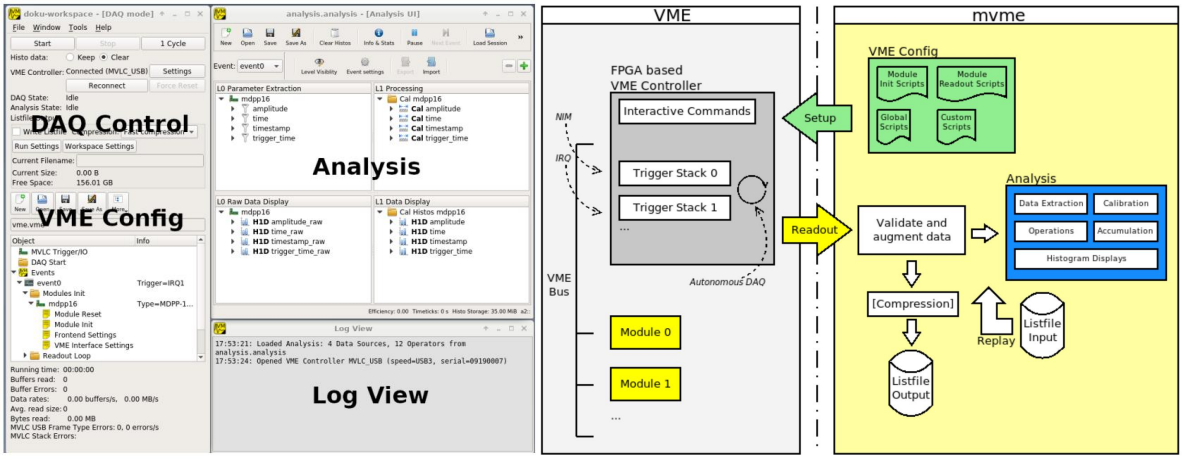

Fig. 4. (Color online) The MVME Software GUI Window and Block Diagram.

III. UNCERTAINTY ANALYSIS OF FED ARRAY

In the photoneutron cross section measurement, the main uncertainty origins from three factors: the fidelity of the incident gamma energy spectrum, uncertainty of neutron counts, the thickness and density of the target. The uncertainty of neutron counts includes its statistical uncertainty, the uncertainty caused by neutron counts extraction algorithm, and FED systematic uncertainty in efficiency. The FED systematic uncertainty is affected by high voltage setting, target position, acquisition system setting, and detector systematic fluctuation. A detailed study on the systematic uncertainty of the FED was conducted using a ^{252}Cf source with neutron emitting rate of 361.3 $\pm$ 10.8 counts/s. The FED was aligned in the experimental hutch to keep the same environment background as the online experiment. Figure 5(a) shows a typical pulse height spectrum measured by one of the ^{3}He counters in FED. Figure 5(b) shows the simulated neutron energy distribution from ^{252}Cf standard neutron source.

The ^{3}He counters operated in proportional region where the detector efficiency has a weak dependence on the high voltage. The detector efficiency for each ring has been tested at a series of high voltages, with each voltage setting tested for 1 hour. Finally, the optimal operating voltages were determined to be 950 V for Ring-1 and 1050 V for Ring-2 and Ring-3. The total detector efficiency are 41.92$\pm$1.25%, 42.10$\pm$1.25%, and 41.91$\pm$1.25% (statistical error only) at the high voltage deviations of -50 V, 0 V, 50 V, respectively. The detector efficiency changes little with a 50 V shift in high voltage. Assuming a linear dependence of the detector efficiency on high voltage, the detector systematic uncertainty caused by high voltage is 0.02% since the CAEN A1589 allows for less than 1 V voltage deviation.

The target position uncertainty was investigated by moving the ^{252}Cf source along the central tunnel of the FED moderator. The dependence of detector efficiency on the source position is shown in Fig. 5(d). The asymmetry of the efficiency distribution is evident due to the asymmetrical detector construction. However, the efficiency changes little when the source is moved a small distance around the center. The contribution to the systematic uncertainty from the source position is 0.10% with a 1 cm deviation.

In addition to the uncertainties mentioned above, deviations may also arise due to the parameters set in the data acquisition system. The fine adjustment of the key parameters and the resulting detector efficiencies are listed in Table 1. A set of reliable parameters that have been proven to be effective in signal amplification and have a weak correlation with the detector efficiency.After a long-term continuous measurement, the entire detector system has been verified to be stable, and the efficiency fluctuation has been measured to be 0.26%. Table 1 summarizes the upper limits of the uncertainties for the detector system. The uncertainty caused by the maximum deviation (1 V) of the high voltage is 0.02%. The efficiency uncertainty caused by the source position bias is 0.10%, assuming a maximum deviation of 1 cm between the source position and the geometric center. The total systematic uncertainty of the FED is 3.02%, obtained by quadratically summing the uncertainties in Table 1 with the ^{252}Cf activity uncertainty of 3.0%.

Figure 3(a) also shows the Geant4 simulated efficiency curve, which the detector construction described in Fig. 2. The total detector efficiency increases from 35.64% at 50 keV to 42.32% at 1.65 MeV and falls slowly to 40.69% at 3

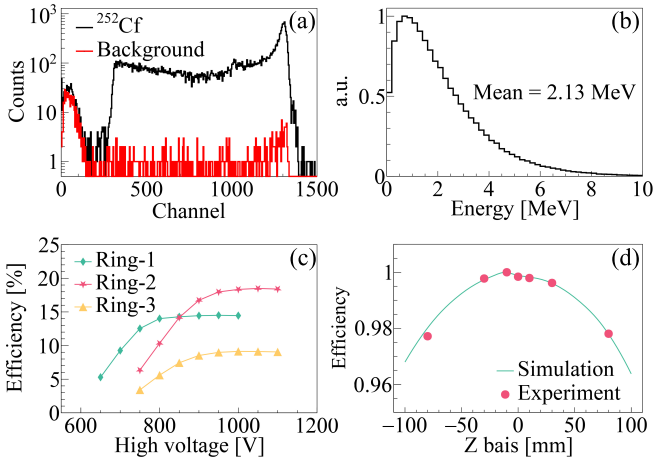

Fig. 5. (a) A typical spectrum with ^{252}Cf neutron source (black line) and the environment background (red line). (b) The simulated neutron energy distribution form ^{252}Cf. (c) The detector efficiency for 3 rings as the function of high voltage. (d) Detector efficiency as the function of source position along the FED center tunnel.

TABLE 1. The systematic uncertainty of the FED array.

Uncertainty Factors	Value
High voltage	0.02%
Preset DAQ parameters	0.17%
Target position bias	0.10%
Efficiency fluctuation	0.26%
^{252}Cf activity uncertainty	3.0%
Total uncertainty	3.02%

MeV for neutrons with energy follows Maxwell-Boltzmann distribution. The efficiency calibrated by ^{252}Cf source, 42.10±1.25%, is marked on the curve at 2.13 MeV, the averaged energy of ^{252}Cf neutron spectrum. In the experiment, the average neutron energy is derived from the Ring-Ratio (RR) technique [28–31], which is indicated by the ratio of outer Ring to inner Ring, as illustrated in Fig. 3(b). The RR technique only provides an average energy for reference, which may differ from the actual value. However, due to the property of flat efficiency profile, the difference between the calculated and the actual detector efficiency is not significant.

IV. PHOTONEUTRON CROSS SECTION DATA ANALYSIS

The photoneutron cross section is defined as

$$\int_{S_n}^{E_{max}} n_\gamma(E_\gamma)\sigma_{\gamma n}(E_\gamma)\mathrm{d}E_\gamma = \frac{N_n}{N_t N_\gamma \xi \epsilon_n g}. \quad (1)$$

where, the $n_\gamma(E_\gamma)$ is the normalized energy distribution of the incident γ-rays. The $\sigma_{\gamma n}(E_\gamma)$ is the monochromatic cross section which will be determined. N_n is the number of detected photoneutrons. N_γ is the number of γ rays incident on the target. ϵ_n represents the average detector efficiency given by the RR technique. N_t is the number of target nuclear per unit area. $\xi = (1-e^{-\mu t})/(\mu t)$ is a correction factor for target self-attenuation. μ is the attenuation coefficient for γ rays. t is the target thickness. g is the fraction of the gamma flux above the S_n,

$$g = \frac{\int_{S_n}^{E_{max}} n_\gamma(E_\gamma)\mathrm{d}E_\gamma}{\int_0^{E_{max}} n_\gamma(E_\gamma)\mathrm{d}E_\gamma}. \quad (2)$$

A. Data preprocessing

The N_n and the N_γ are the measurement parameters from FED and BGO (or $LaBr_3$) detector. In the data analysis program, the γ-ray spectra incident on the target have been solved, which not only yields N_γ, but also provides the normalized gamma energy spectra, which are essential for solving monochromatic cross sections. N_n can be extracted by analyzing the time distribution of the signals, since the laser is in pulse form and the DAQ records the timestamp of each signal from the detector. This section introduces the method for extracting N_n and N_γ.

The SSRF operates in top-up mode, with the storage ring circumference being 432 meters, and it takes 1.44 μs for electrons to complete one revolution. The electron beam is divided into 720 buckets, with approximately 500 buckets loaded with electron bunches. These electron bunches are divided into 4 groups, with a 2 ns interval between adjacent electron bunches within each group. The CO_2 laser is operated in pulsed mode, using a dedicated trigger for the laser output. Typically, the laser operates at a power of 5 W, corresponding to a period of 1000 μs and a pulse width of 50 μs. Figure 6 is a schematic diagram of the time distribution of the laser and electron beam.

The laser period is set to be 1000 μs. However, the actual period is not exactly equal to 1000 μs, and there is a slow variation. Fortunately, this variation does not affect the data analysis. Therefore, it is necessary to analyze the precise period for each file to obtain the time distribution of signals within a laser period. The precise period is determined by scanning over a certain range of laser periods. The optimal period is the one that leads to the narrowest FWHM of the time distribution spectrum as shown in Fig. 7(a). The background is subtracted using the time distribution at this optimal period. N_n can be directly extracted from the neutron time distribution spectrum (see Fig. 7(c)). The γ-ray time distribution spectrum (Fig. 7(b)) is used to extract the LCS γ spectrum from the electron bremsstrahlung background, known as the LCS detector response spectrum (the orange line in Fig. 7(d)). Then, the incident energy spectrum on the detector is calculated using the direct unfolding method, for details see article [16]. Figure 8 shows the incident gamma spectrum obtained from the direct unfolding method (red solid line), the detector response spectrum (blue dashed line), and the reconstructed spectrum (black solid line). Subsequently, the energy spectrum incident on the target is calculated based on the thickness and attenuation coefficient of the attenuator (Cu) and the thickness and attenuation coefficient of the target. The integral of

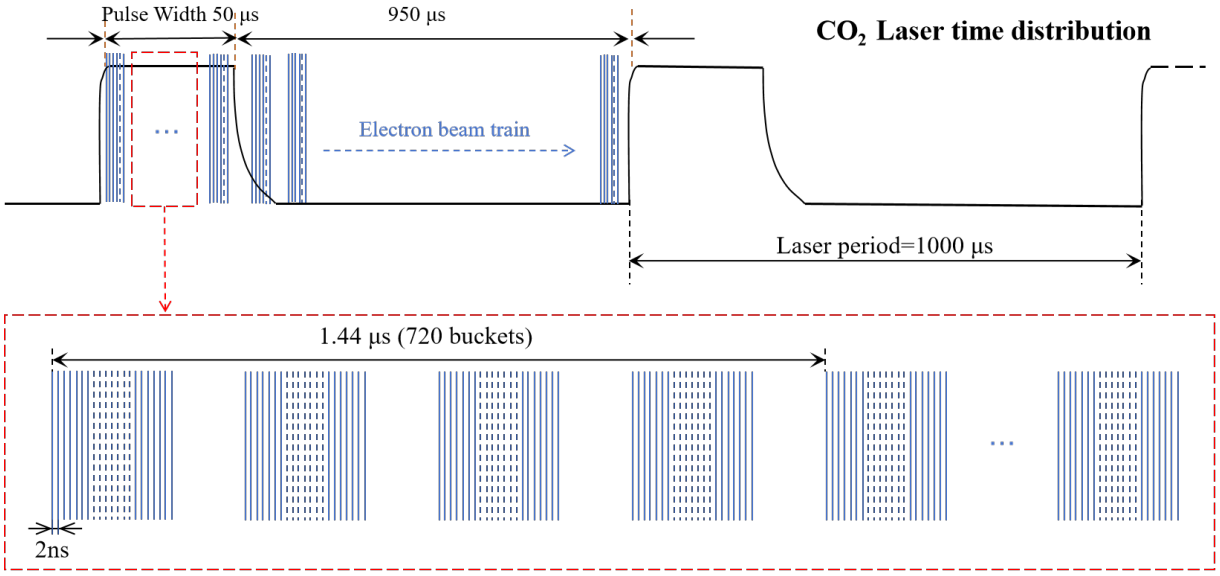

Fig. 6. (Color online) The time distribution of laser and electron beam in SLEGS.

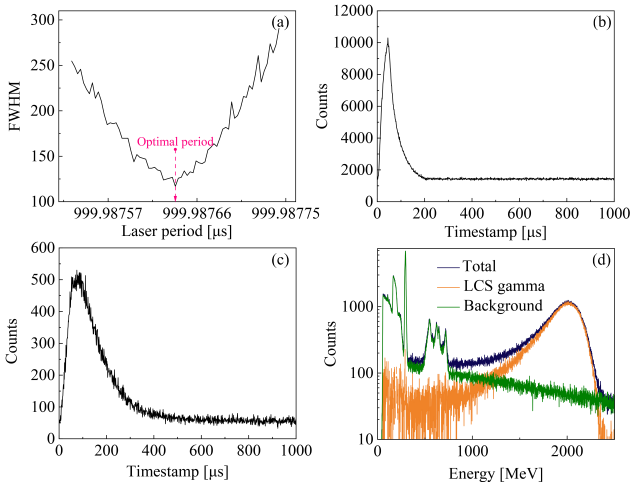

Fig. 7. (Color online) (a) A scanning of FWHM for the optimal laser period. (b) The γ-ray time distribution at the optimal laser period. (c) The neutron time distribution at the optimal laser period. (d) The LCS detector response spectrum (orange line) is calculated by subtracting the bremsstrahlung background (green line) from the total detector response spectrum (black line).

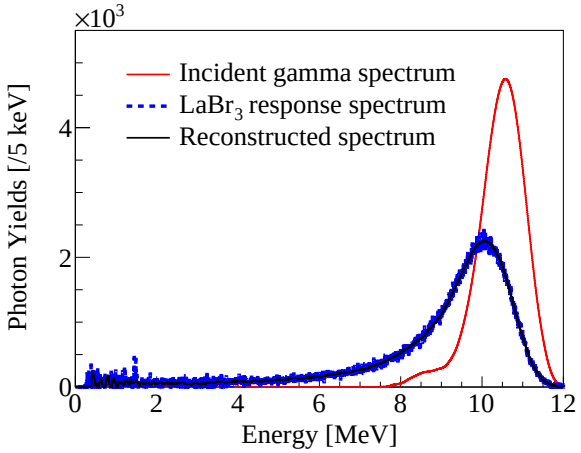

Fig. 8. (Color online) The incident gamma spectrum (red solid line) through the direct unfolding method and its corresponding response spectrum (blue dashed line). The reconstructed spectrum (black solid line) is derived by folding the incident gamma spectrum with the detector response matrix.

the gamma energy spectrum incident on the target yields N_γ.

In the N_n extraction algorithm, each ring is analyzed as an independent unit, which is essential because the RR technique requires the count of Ring-3 and Ring-1. As indicated by the colored arrows in Fig. 3, one can first obtain the value of Ring-3 divided by Ring-1 (cyan dot). Based on the RR curve, the average neutron energy is obtained (blue dot). Finally, the average neutron efficiency ϵ_n is determined from the efficiency curve (red dot). The right side of Equation 1 is referred to as monochromatic approximation cross section (also folded cross section), since the incident gamma is quasi-monochromatic.

B. Monochromatic Photoneutron cross section

The monochromatic approximation cross section is an averaged cross section with the weight of normalized in incident gamma spectrum. In this section, the algorithm for extracting monochromatic cross sections is introduced. The monochromatic approximation cross section can be expressed as

$$\sigma_{\mathrm{f}} = \mathbf{D}\sigma. \tag{3}$$

The $\sigma_{\rm f}$ is a monochromatic approximation cross section array. Each element in $\sigma_{\rm f}$ is the monochromatic approximation cross section measured at discrete beam energies (E_γ). The σ is an array consisting of monochromatic cross sections. The matrix **D** is composed of normalized incident gamma energy distributions from $S_{\rm n}$ to $E_{\rm max}$. Equation 4 is the expansion form of Eq.3. The number of rows (N) in **D** corresponds to the number of discrete beam energies, while the number of columns (M) corresponds to the number of bins in the incident gamma spectrum from $S_{\rm n}$ to $E_{\rm max}$.

$$\begin{pmatrix} \sigma_1 \\ \sigma_2 \\ \vdots \\ \sigma_N \end{pmatrix}_{\rm f} = \begin{pmatrix} D_{11} & D_{12} & \dots & D_{1M} \\ D_{21} & D_{22} & \dots & D_{2M} \\ \vdots & \vdots & \ddots & \vdots \\ D_{N1} & D_{N2} & \dots & D_{NM} \end{pmatrix} \begin{pmatrix} \sigma_1 \\ \sigma_2 \\ \vdots \\ \vdots \\ \sigma_M \end{pmatrix}. \quad (4)$$

An unfolding iteration method is used to extract the monochromatic cross section σ:

(1) First, assign a value to σ, for example, $[1, 1, 1, ..., 1]^T$, denoted as σ^0 in the first iteration, and substitute it into Eq. 3 to obtain $\sigma_{\rm f}^0$.

(2) Then, based on the difference between $\sigma_{\rm exp}$ and $\sigma_{\rm f}^0$, adjust σ^0 to obtain σ^1.

$$\sigma^1 = \sigma^0 + (\sigma_{\rm exp} - \sigma_{\rm f}^0). \quad (5)$$

It is worth noting that the dimension of σ^0 (M) is much larger than that of $\sigma_{\rm exp}$ and $\sigma_{\rm f}^0$ (N). To perform Eq. 5, it is necessary to expand the dimensions of $\sigma_{\rm exp}$ and $\sigma_{\rm f}^0$ to M.

(3) The i-th iteration follows the same algorithm, given by

$$\sigma_{\rm f}^i = \mathbf{D}\sigma^i, \quad (6)$$

$$\sigma^{i+1} = \sigma^i + (\sigma_{\rm exp} - \sigma_{\rm f}^i). \quad (7)$$

The χ^2 between $\sigma_{\rm exp}$ and $\sigma_{\rm f}^{i+1}$ is recorded in each iteration. The iteration procedure stops when χ^2 converges.

TECHNICAL VALIDATION

Figure 9 presents a comparison of monochromatic cross-sections for ^{197}Au and ^{159}Tb of the SLEGS experiment with data obtained from other laboratories. The SLEGS data have been submitted to Science Bulletin [17], and the data shown here are to illustrate the rationality of the data processing method.

The whole process of photonuclear neutron cross section measurement and data analysis is displayed and summered in Fig. 10, where the methodology for measuring the (γ,2n) cross section is under development (colored in gray). A batch of photoneutron experiments at SLEGS has been completed, and the measurement data is being analyzed, to be progressively published for user access and verification, particularly for photonuclear data compilation and evaluation in the Chinese nuclear database (CENDL/PD).

USAGE NOTES

1. Photoneutron cross-sectional data is one of many reaction channels of photonuclear reactions. SLEGS is capable of performing (γ, 1n) cross section measurements. However, the methodology for cross section measurements with (γ, 2n) reaction is still under development. Due to the constraints on the maximum energy available in SLEGS, reactions beyond (γ, 2n) are not allowed.

2. The quasi-monochromatic cross section is an average weighted cross section with the weights based on the normalized incident gamma spectra. Consequently, the fine structures in some cross sections may be smoothed out.

3. The (γ, 1n) photoneutron cross section unfolding program can not only extract the monochromatic cross sections at the measured energy points but also provide numerical values for the cross sections within the measured energy range. Additionally, it is capable of making predictions for a certain range beyond the measured energy limits.

4. The RAW data of ^{197}Au(γ, 1n) and ^{159}Tb(γ, 1n) has been uploaded to Science Data Bank. [32, 33] Also, the monochromatic cross section data can be obtained through [34]. The Description section of the raw data set is a list that describes the data generated by MVME and the corresponding data generated by DT5730B, along with the corresponding attenuation thickness. From this, neutron counts and gamma counts (gamma spectra) can be extracted. The monochromatic cross section can be found in the Description section of [34].

CODE AVAILABILITY

The photoneutron cross sectional data processing program mainly consists of the following components: a program for converting binary data generated by MVME into CERN ROOT format, a photoneutron count extraction program, an LCS gamma extraction program, an incident gamma spectrum unfolding program, a quasi-monochromatic cross section calculation program, and a monochromatic cross section extraction program. These programs are not available online. SLEGS will provide the programs and user instructions to users who apply for photoneutron cross section measurement experiments.

ACKNOWLEDGMENTS

The authors would like to thank the Shanghai Light Source Accelerator and Beam Line Engineering Department for their technical support, and the cooperative research units for their support and assistance.

AUTHOR CONTRIBUTIONS STATEMENT

Hongwei Wang and Gongtao Fan led the construction of the SLEGS beamline and experimental station. Zirui Hao and

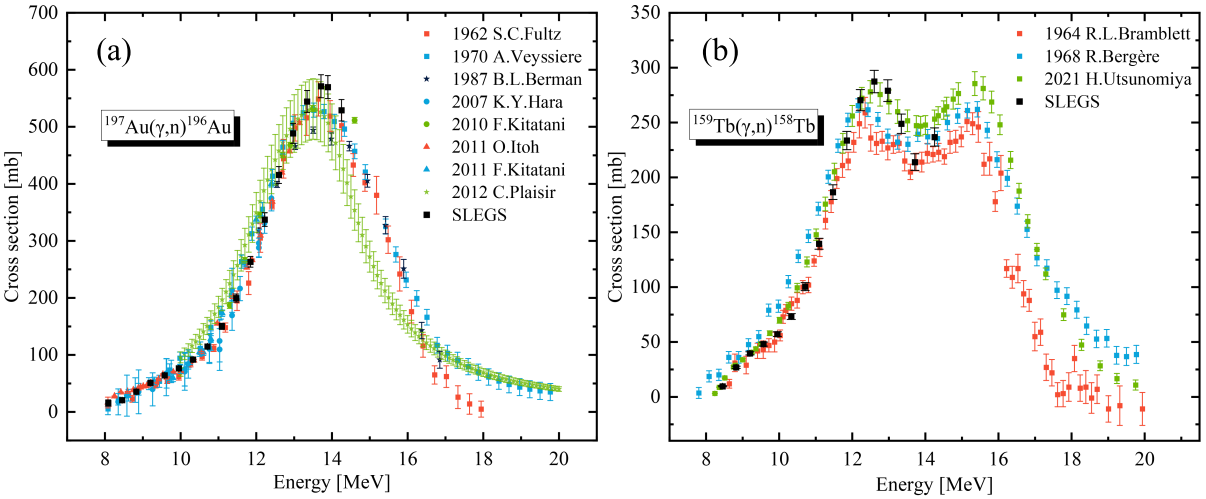

Fig. 9. (Color online) The measured photoneutron cross section of (a) ^{197}Au and (b) ^{159}Tb at SLEGS.

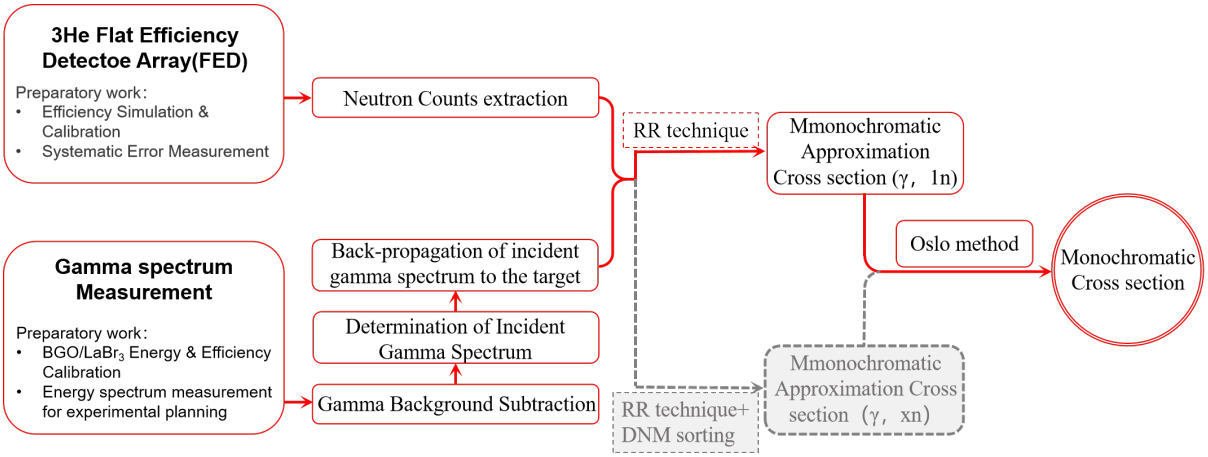

Fig. 10. (Color online) The photoneutron cross section measurement method in SLEGS. The preliminary work including offline testing of the FED and γ beam measurements are also depicted in the diagram. The methodology for measuring the (γ, 2n) cross section is under development, which is in gray color.

Longxiang Liu carried out FED experimental methodological research and measurement. Hanghua Xu, Yue Zhang, Yuxuan Yang, Sheng Jin, Kaijie Chen, Zhicai Li, Pu Jiao, Qiankun Sun, Mengdie Zhou, Shan Ye, Zhenwei Wang, Mengke Xu, Xiangfei Wang and Yulong Shen performed experiment. Zirui Hao, Gongtao Fan and Hongwei Wang contributed to the writing, review, and editing of the manuscript. All authors discussed the results and reviewed the manuscript.

COMPETING INTERESTS

The authors declare that they have no conflict of interest.

FIGURES & TABLES

The main parameters used for the measurements of the SLEGS photoneutron cross-section are listed in Table 2.

There are two types of photoneutron measurement spectrometers of FED and TOF, and the methodology of the TOF spectrometer is being studied. In addition, SLEGS has built nuclear resonance fluorescence (RNF) and light charged particle (LCP) spectrometers; their datasets also have their own characteristics and will be demonstrated in future studies.

REFERENCES

TABLE 2. The main parameters of SLEGS and FED array for photoneutron cross section measurement.

Parameter Name/Units	Value or Mode
Electron Energy/GeV	3.5
Beam Current/mA	180-220
SSRF Operation Mode	Topup or Decay
CO_2 Laser Power/W	5-20-100(Adjustable)
Duty cycle/us	50/1000(Adjustable)
Coarse Collimator Diameter/mm	0-5,8,10,20,30(Adjustable)
Fine Collimator Diameter/mm	0-30(Adjustable)
Three-hole Collimator Diameter/mm	1,2,3
Copper internal Attenuator/mm	0-640 (Adjustable)
Copper external Attenuator/mm	0-1000(Adjustable)
X-rays spot Monitor	MiniPIX [27]
γ-rays spot Monitor	Gamma Spot Monitor- GSM
Gamma Beam Flux Monitor	$LaBr_3$ or BGO
Gamma Beam Flux DAQ	CAEN CoMPASS
Photoneutron Detector Array	FED
FED array neutron data DAQ	Mesytec MVME

[1] S.S.Dietrich,B.L.Berman, Atlas of photoneutron cross sections obtained with monoenergetic photons. Atom. Data Nucl. Data Tables **38**, 199–338 (1988). doi:10.1016/0092-640X(88)90033-2

[2] A.J.Koning,D.Rochman,J.C.Sublet, et al., TENDL: Complete nuclear data library for innovative nuclear science and technology. Nucl. Data Sheets **155**, 1–55 (2019). doi:10.1016/j.nds.2019.01.002

[3] D.A.Brown, M.B.Chadwick,R.Capote, et al., ENDF/B-VIII.0:The 8th major release of the nuclear reaction data library with CIELO-project cross sections, new standards and thermal scattering data. Nucl. Data Sheets **148**, 1–142 (2018). doi:10.1016/j.nds.2018.02.001

[4] O.Iwamoto,N.Iwamoto,S.Kunieda, et al., Japanese evaluated nuclear data library version 5: JENDL-5. J. Nucl. Sci. Technol. **60**, 1–60 (2023). doi.org/10.1080/00223131.2022.2141903

[5] Z.Ge,R.Xu,H.Wu,et al., CENDL-3.2:The new version of Chinese general purpose evaluated nuclear data library**239** of EPJ Web of Conferences,(2020). doi:10.1051/epjconf/202023909001

[6] A.G.Kazakov,T.Y.Ekatova,J.S.Babenya, Photonuclear production of medical radiometals: a review of experimental studies. J. Radioanal. Nucl. Chem. **328**, 493–505 (2021). doi:10.1007/s10967-021-07683-2

[7] Z.Hao,G.Fan,H.Wang,et al., Collimator system of SLEGS beamline at Shanghai Light Source. Nuclear Instruments and Methods in Physics Research Section A: Accelerators, Spectrometers, Detectors and Associated Equipment **1013**, 165638 (2021). doi:10.1016/j.nima.2021.165638

[8] H.Xu,G.Fan,H.Wang,et al., Interaction chamber for laser Compton slant-scattering in SLEGS beamline at Shanghai Light Source. Nuclear Instruments and Methods in Physics Research Section A: Accelerators, Spectrometers, Detectors and Associated Equipment **1033**, 166742 (2022). doi:10.1016/j.nima.2022.166742

[9] Hongwei Wang, Gongtao Fan, Longxiang Liu et al., Development and Prospect of Shanghai Laser Compton Scattering Gamma Source. Nuclear Physics Review(In Chinese) **37** (2020). doi:10.11804/NuclPhysRev.37.2019043

[10] H.W.Wang,G.T.Fan,L.X.Liu, et al., Commissioning of laser electron gamma beamline SLEGS at SSRF. Nucl. Sci. Tech. , 033 (2022). doi:10.1007/s41365-022-01076-0

[11] K.J.Chen,L.X.Liu,Z.R.Hao, et al., Simulation and test of the SLEGS TOF spectrometer at SSRF. Nucl. Sci. Tech. **34** (2023). doi:10.1007/s41365-023-01194-3

[12] X.Pang,B.H.Sun,L.H.Zhu, et al., Progress of photonuclear cross sections for medical radioisotope production at the SLEGS energy domain. Nucl. Sci. Tech. **34** (2023). doi:10.1007/s41365-023-01339-4

[13] Z.C.Li,Y.Yang, Z.W.Cao, et al., Effective extraction of photoneutron cross-section distribution using gamma activation and reaction yield ratio method. Nucl. Sci. Tech. **34** (2023). doi:10.1007/s41365-023-01330-z

[14] L.X.Liu,H.W.Wang,G.T.Fan, et al., The SLEGS beamline of SSRF. Nucl. Sci. Tech. **35** (2024). doi:10.1007/s41365-024-01469-3

[15] Z.R.Hao,H.H.Xu,G.T.Fan, et al., Gamma spot monitor at SLEGS beamline. Nucl. Instrum. Methods Phys. Res. Sect. A-Accel. Spectrom. Dect. Assoc. Equip. **1068** (2024). doi:10.1016/j.nima.2024.169748

[16] L.Liu,H.Utsunomiya,G.Fan, et al., Energy profile of laser Compton slant-scattering γ-ray beams determined by direct unfolding of total-energy responses of a BGO detector. Nucl. Instrum. Methods Phys. Res. Sect. A-Accel. Spectrom. Dect. Assoc. Equip. **1063**, 169314 (2024). doi:10.1016/j.nima.2024.169314

[17] Z.R.Hao,G.T.Fan, et al., The day-one experiment at SLEGS: systematic measurement of the (γ,1n) cross sections on ^{197}Au and ^{159}Tb for resolving existing data discrepancies. Science Bulletin. Submitted.

[18] Zirui Hao,Gongtao Fan,Longxiang Liu, et al., Design and simulation of 4π flat-efficiency ^{3}He neutron detector array. Nuclear Techniques (in Chinese) **43**, 110501–110501 (2020). doi:10.11889/j.0253-3219.2020.hjs.43.110501

[19] DIAMOND C/Cx Series, low power CO_2 Lasers, https://www.coherent.com/lasers/co2/diamond-c-cx-series

[20] Bismuth germanate(BGO), Shanghai SICCAS high technology corporation, http://www.siccas.com/bgo.aspx?pId=42

[21] Lanthanum Bromide($LaBr_3$), https://www.luxiumsolutions.com/radiation-detection-scintillators/crystal-scintillators/lanthanum-bromide-labr3

[22] ROOT: analyzing petabytes of data, scientifically. https://root.cern.ch/

[23] CAEN A1589, 8 Channel $\pm$ 2.5 kV/500 µA 4 Quadrant Bipolar Board, https://www.caen.it/products/a1589/

[24] CAEN SY4527LC, Universal Multichannel Power Supply System (Low Cost), https://www.caen.it/products/sy4527lc/

[25] Mesytec MDPP-16, fast high resolution time and amplitude digitizer, https://www.mesytec.com/products/nuclear-physics/MDPP-16.html

[26] Mesytec MVME - Mesytec VME Data Acquisition, https://www.mesytec.com/downloads/mvme.html

[27] Advacam MiniPIX TPX, a miniaturized and low-power radiation camera, https://advacam.com/camera/minipix-tpx3/

[28] B.L.Berman,J.T.Caldwell,R.R.Harvey, et al., Photoneutron Cross Sections for ^{90}Zr, ^{91}Zr, ^{92}Zr, ^{94}Zr, and ^{89}Y. Physical Review **162**, 1098 (1967). doi:10.1103/PhysRev.162.1098

[29] B.L.Berman,S.C.Fultz, Measurements of the giant dipole resonance with monoenergetic photons. Rev.Mod.Phys. **47**, 713–761 (1975). doi:10.1103/RevModPhys.47.713

[30] O.Itoh, H.Utsunomiya, H.Akimune, et al., Photoneutron Cross Sections for Au Revisited: Measurements with Laser Compton Scattering γ-Rays and Data Reduction by a Least-Squares Method. J. Nucl. Sci. Technol. **48**, 834–840 (2011). doi:10.3327/jnst.48.834

[31] I.Gheorghe, H.Utsunomiya, S.Katayama, et al., Photoneutron cross-section measurements in the ^{209}Bi (γ, xn) reaction with a new method of direct neutron-multiplicity sorting. Phys. Rev. C **96**, 044604 (2017). doi:10.1103/PhysRevC.96.044604

[32] hao, Liu Longxiang, Zhang Yue, et al., 197Au(,n) cross section RAW data[DS/OL]. V1. Science Data Bank, 2025[2025-01-07]. doi:10.57760/sciencedb.19543

[33] Hao Zirui, Liu Longxiang, Zhang Yue, et al., 159Tb(,n) photoneutron cross section RAW data[DS/OL]. V1. Science Data Bank, 2025[2025-01-07]. doi:10.57760/sciencedb.19552

[34] Hao Zirui, Liu Longxiang, Zhang Yue, et al., 197Au(,n) and 159Tb(,n) cross section[DS/OL]. V1. Science Data Bank, 2025[2025-01-07]. doi:10.57760/sciencedb.19582